Journal of
Composites Science

MDPI

Article

A Systematic Approach to Determine the Cutting Parameters of AM Green Zirconia in Finish Milling

Laurent Spitaels, Hugo Dantinne, Julien Bossu, Edouard Rivière-Lorphèvre and François Ducobu *

Machine Design and Production Engineering Lab, Research Institute for Science and Material Engineering, UMONS, 7000 Mons, Belgium
* Correspondence: Francois.Ducobu@umons.ac.be

Abstract: Additive manufacturing (AM) opens new possibilities of obtaining ceramic green parts with a tailored complex design at low cost. Meeting the requirements of highly demanding industries (aeronautical and biomedical, for example) is still challenging, even for machining. Hybrid machines can solve this problem by combining the advantages of both additive and subtractive processes. However, little information is currently available to determine the milling parameters of additively fabricated ceramic green parts. This article proposes a systematic approach to experimentally determine the cutting parameters of green AM zirconia parts. Three tools, one dedicated to thermoplastics, one to composites, and a universal tool, were tested. The tool–material couple standard (NF E 66-520-5) was followed. The lower cost and repeatable generation of smooth surfaces (Ra $<$ 1.6 µm) without material pull-out were the main goals of the study. The universal tool showed few repeatable working points without material pull-out, while the two other tools gave satisfying results. The thermoplastic tool ensured repeatable results of Ra $<$ 0.8 µm at a four times lower cost than the composite tool. Moreover, it exhibited a larger chip thickness range (from 0.003 mm to 0.036 mm). Nevertheless, it generated an uncut zone that must be considered when planning the milling operations.

Keywords: hybrid machine; green ceramic; milling; additive manufacturing; material extrusion; finishing operations

Citation: Spitaels, L.; Dantinne, H.; Bossu, J.; Rivière-Lorphèvre, E.; Ducobu, F. A Systematic Approach to Determine the Cutting Parameters of AM Green Zirconia in Finish Milling. *J. Compos. Sci.* **2023**, *7*, 112. https://doi.org/10.3390/jcs7030112

Academic Editor: Yuan Chen

Received: 9 February 2023
Revised: 24 February 2023
Accepted: 7 March 2023
Published: 10 March 2023

1. Introduction

1.1. Context

Ceramics and advanced ceramics, such as zirconia, are key materials in a wide range of sectors, such as the electrical, mechanical, chemical, and biomedical industries [1,2]. From the large choice offered by the ceramic materials, 3Y-TZP (Yttrium Tetragonal Zirconia Polycrystal) exhibits very interesting mechanical properties. Indeed, its fracture toughness (4–12 MPa$\sqrt{m}$) and flexural strength (500–1800 MPa) are among the highest available in commercial ceramics [3]. These properties, added to its high chemical resistance, make zirconia very attractive for the oil and gas, biomedical and tooling sectors [1,3,4].

The conventional processing route to manufacture ceramics is usually made of four main steps: the powder synthesis, the shaping of the part (obtention of a green body), and its debinding (obtention of a brown body) and sintering (obtention of a white body) operations. However, for demanding applications (such as contact, for example), a very good surface topography (Ra $<$ 1.6 µm) can be required, and this leads to additional finishing operations performed after sintering (usually consisting of polishing, grinding, or lapping) [3]. However, these operations can represent up to 80% of the total production costs of the part [3]. Indeed, when the finishing operation is performed on the sintered part, it has already acquired the final material properties and requires dedicated tools and careful operators. Moreover, machining operations can lead to micro-cracks and surface defects that decrease the final part's properties [4]. Machining the part at the green stage (just after

its shaping) is, consequently, an interesting solution. Indeed, at the green state, the part mostly exhibits the mechanical properties of its binder, which is usually a thermoplastic polymer [5]. Consequently, green machining operations are less expensive and easier to perform while reducing the risk of generating macro defects like cracks, which can lead to the premature failure of the part during its service [4,5].

One of the major drawbacks of the conventional ceramic production route is the impossibility of generating complex designs with, for example, dedicated pore size and interconnectivity or a very fine structure [2,6]. Moreover, the costs to produce a single part with a non-standard design are too high [7], discounting the possibility of serial and personalized production as in Industry 4.0 [8]. Conventional processes are then only economically viable for intermediate, and large series production [3]. Such characteristics (complex tailored design) are required for specific applications, such as in the biomedical sector [7,9]. Non-conventional processes, such as additive manufacturing (AM), are bringing an answer to these problems and offer great hopes and promises [2,10]. Additive processes, in opposition to subtractive processes, enable the production of geometrically complex parts in near-net shapes [11]. Moreover, these processes allow the generation of parts with less material than conventional processes (than in machining, for example) [11] and without the need to invest in costly pieces of equipment specific to a single part design, such as moulds for Ceramic Injection Moulding (CIM) and Metal Injection Moulding (MIM) [2,6].

In the seven families of AM processes classified by the ISO/ASTM 52900 standard, material extrusion is one of the most promising in a ten-year horizon, according to a SmarTech Analysis of 2018 [12]. Indeed, this technology allows the relatively low-cost fabrication of ceramics and metal parts through the use of highly-filled polymer filaments containing ceramic or metal particles [2,8]. The material extrusion method using a fused filament is named Fused Deposition Modelling (FDM) [7]. One of the major limitations of the AM processes is their feedstock availability, and cost [8]. The pellets of the Powder Injection Moulding (PIM) processes can solve this issue since they have been used since the 1970s in the industry [13]. The processes using the FDM method with pellets are named Pellet Additive Manufacturing (PAM). This kind of process does not require high capital expenditure investment (CAPEX), is compatible with every material used in the conventional injection processes (even metals and ceramics), and can be inserted inside an existing workshop using already available MIM or CIM machines [14]. The PAM process produces parts in a green state. Indeed, the ceramic powder in the pellets is mixed with an organic or inorganic binder [9]. The PAM process is referred to as indirect since the shaping and sintering operations are decoupled [9]. The part shaped by the PAM process will then require debinding and sintering steps to achieve its final density and mechanical properties.

Even if the PAM process allows the generation of complex designs impossible to obtain using the conventional ceramic forming processes, these exhibit rough surfaces compared to the other AM processes due to the inherent staircase effect [8,15]. The high arithmetic roughness (from 9 µm to 40 µm [16]) reduces the fatigue resistance of the parts, and their tribological properties [17,18]. Some conventional machining operations (such as turning and milling) can solve the problem but require simple designs [5,19]. Indeed, complex parts exhibiting an internal lattice structure cannot be machined even with 5-axis machining since the inner surfaces of the part are unattainable by the cutting tool. Moreover, when applied to fully dense parts obtained after sintering, the machining operations are difficult and very expensive, as explained earlier [19].

All these reasons motivate the development of methods combining the advantages of the AM processes and machining. Such machines are called hybrid [5,20] and are currently subject to a strong industrial interest [21]. Commercial hybrid machines combining additive and subtractive processes already exist. They allow the generation of metal parts with Direct Energy Deposition (DED) or Selective Laser Sintering (SLS) [5,20]. However, their price is very high since the machining operations are made in a dense part, then requiring a robust and complex construction while dealing with low material removal rates and challenging tool wear. A solution to this problem is to machine the part when it is in a

green state [5,22]. Indeed, the part in the green state requires less energy to be machined than dense parts since it behaves as a pseudo-plastic material [5,22]. This effect, added to lower thermal stresses, allow the reduction of tool wear and consequently avoids the need for expensive tools [5].

In the case of ceramic parts, hybrid machines are not yet commercialised. Moreover, as announced in a recent review [19], there is a lack of data for the machining of materials shaped by additive manufacturing, except for highly used alloys, such as Ti6Al4V. The determination of the most suitable cutting parameters in green ceramics obtained using the PAM process will then allow the fabrication of a hybrid machine able to produce ceramic parts with tight tolerances and smooth surface topography to be foreseen.

1.2. NF E 66-520-5 Standard

The cutting parameters of ductile materials can be experimentally determined using the tool–material couple standard NF E 66-520-5 [23]. This standard provides a method using mainly the specific cutting energy to quantify the ability of a tool (generation of an appropriate surface topography while avoiding catastrophic damage mode of the tool) to realise machining operations on a specific material. The standard also advices to take into account the surface topography when the tool will be used for finishing operations, as in this work.

Green ceramics do not behave as ductile materials. Consequently, the standard cannot be directly applied. However, recent papers [4,22] have already used the standard to obtain ranges of cutting parameters and to compare the behaviour of a dedicated material to ductile materials. This paper uses the tool–material couple standard as a general guide to determine the suitable cutting parameters for a determined tool. As described in the standard dedicated to milling operations, four cutting parameters were used: the cutting speed (v_c), the feed per tooth (f_z), the depth of cut (a_p), and the radial depth of cut (a_e).

The standard proposes to perform six different experiments [23]:

- Selection of a stable operating point (qualification test);
- Determination of $v_{c,min}$;
- Determination of minimal and maximal chip thickness ($h_{min} - h_{max}$);
- Determination of limiting data;
- Wear tests;
- Tests to determine the auxiliary parameters.

The experiments of the standard allow the determination of the working range for $v_{c,min}$, f_z, a_p, and a_e. When machining is performed with a tool within its working range, it is repeatable, i.e., two different machining operations conducted with the same parameters lead to the same results in terms of specific cutting energy (the power needed to remove a given volume of material) and surface topography. Achieving this repeatability is required to foresee reliable finishing operations.

1.3. Motivation and Objective of the Paper

Even though green ceramic machining has been performed for decades [3], no standardised methods exist to determine the appropriate cutting conditions for such a material. The tool–material couple standard can be a relevant guide, even though it was designed for ductile materials as demonstrated in the literature [4,22]. Moreover, the PAM process opens new possibilities in terms of geometrical complexity for ceramic parts thanks to its flexibility of feedstock [7,14]. However, the surface topographies, as well as dimensional and geometrical tolerances generated by this process, still exhibit high arithmetic roughness (Ra $>$ 1.6 µm), which makes them not suitable for contact applications. Finishing the parts using conventional processes, such as milling, is then mandatory.

In this context, the objective of this paper is the determination of suitable cutting parameters for the finishing of green ceramic parts obtained with the PAM process. To guarantee low costs of processing, three standard milling tools were selected. One is dedicated to thermoplastics, another to composites, and the last is suitable for a large set of

materials (universal tool). The tool–material couple standard [23] was used as a guide to establishing the different cutting conditions. This paper is the first to apply a systematic and objective method to determine the cutting parameters of AM green ceramics. The main objectives in terms of surface topography are to ensure Ra $<$ 1.6 µm and a surface without material pull-out.

2. Materials and Methods

2.1. Manufacturing of Parts

The geometry of the parts is a cube on top of a cylinder. The cylinder has a diameter of 15 mm and a height of 15 mm while the cube exhibits dimensions of 20 mm $\times$ 20 mm $\times$ 20 mm. Machining is performed on the cube while the part's fixture is ensured by the cylinder. A fillet of 3 mm links both geometrical entities and decreases the risk of deformation after printing. Figure 1 shows the part's geometry as well as its reference axes. The *Z* axis was set along the cylinder's main axis direction, and the *X* and *Y* axes were aligned with two edges of the cube.

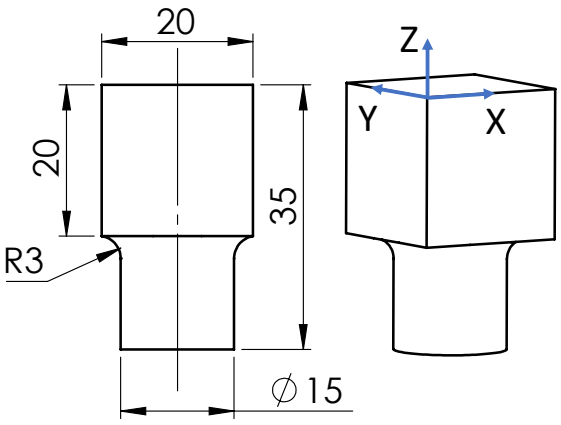

Figure 1. Design of the parts (in mm).

The printing of the parts was performed on a Pollen AM Series MC (Ivry-sur-Seine, France). This PAM printer was fed with K2015 pellets from Inmatec (Rheinbach, Germany). This feedstock is composed of a mix of polyamide binder (15% in mass) and zirconium oxide (85% in mass) partially stabilised with 3 mol% of yttrium oxide (Y_2O_3). The resulting material exhibits a density of 6000 kg/m^3. The zirconium oxide used in the feedstock has a d_{50} of 0.5 µm and comes from the Tosoh Corporation (Tokyo, Japan). This feedstock is developed for the CIM industry and requires a temperature of injection between 110 °C and 150 °C while ensuring a back pressure above 50 bar. After its shaping, the part will require a two-stage debinding before its sintering operation. The first stage is chemical with acetone, while the second is thermal (temperature up to 325 °C). The final sintering operation should be performed at 1400 °C in air. The resulting material has a black colour after its sintering operation.

The printer was used with a 1 mm nozzle diameter. The layer thickness was set at 0.35 mm while the first layer thickness was set at 0.17 mm. The extrusion temperature stood at 165 °C while the build platform temperature was set at 35 °C. An amount of 100% of the infill was selected with a concentric strategy deposition. The build direction was set along the part's Z axis, and the cubic base was the first to be printed. This avoided the use of support. The printing of a part took about 25 min. SolidWorks version 2021 was used to create the CAD file, while Cura version 4.1 generated the sliced file. The STL format was selected to transfer the CAD from SolidWorks to Cura. Figure 2 shows a part after its fabrication, while Figure 3 gives the surface topography obtained. As can be seen in the pictures, the part exhibits a very rough surface topography. Its arithmetic roughness was estimated to be higher than 12.5 µm using a viso-tactile roughness comparator, demonstrating the need for finishing to achieve the required arithmetic roughness.

Figure 2. As built part before milling.

Figure 3. Surface topography of the as built part before milling.

2.2. Milling and Data Acquisition

The milling operations were performed on a Stäubli TX200 (Pfäffikon, Switzerland) fitted with a Teknomotor ATC71 electrospindle (Quero, Italy). The spindle exhibits a maximal power of 7.8 kW and a maximal rotational speed (N) of 24,000 rpm. Figure 4 gives an overview of the cutting configuration.

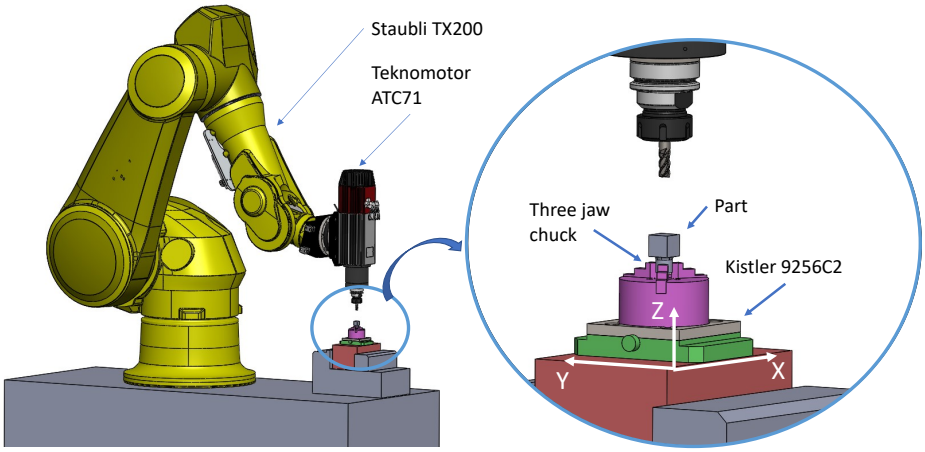

Figure 4. Cutting configuration.

Three different tools with a 6-mm diameter were selected. Their diameter was chosen to ensure a high enough cutting speed since the maximal spindle speed was 24,000 rpm. Table 1 gives the main characteristics of the selected tools, such as their diameter (D), number of teeth (z), maximal axial depth of cut ($a_{p,max}$), supplier reference and relative

price compared to the tool dedicated to the thermoplastics (reference price). In the rest of the paper, and for the sake of simplicity, each tool is called by the material for which it was designed (e.g., thermoplastic tool). The geometry of each tool is shown in Figure 5.

Table 1. Main characteristics of the selected tools.

Type of Tool	D (mm)	z	$a_{p,max}$ (mm)	Price	Supplier/Reference
Thermoplastics	6	3	19	1.00	Hoffmann/209425 6
Composites	6	10	18	3.64	SECO/871060.0-DURA
Universal	6	3	14	1.63	SECO/553060SZ3.0-SIRON

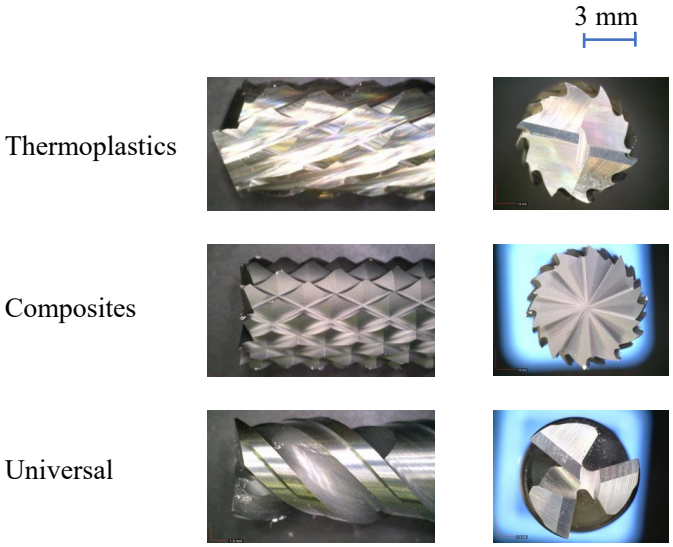

Figure 5. Geometry of the thermoplastic, composite, and universal tools.

The desired cutting parameters were related to the finishing of AM parts. As a consequence, 3 mm axial depth (a_p) and 0.5 mm radial depth of cut (a_e) were selected. Indeed, in finishing operations, only the external layer had to be removed. Straight shoulders were milled on the part along its X axis.

The part was clamped into a three-jaw chuck, itself rigidly attached to a Kistler 9256C2 force sensor (see Figure 4, Winterthur, Switzerland). The cutting forced signals in the X (feed direction), Y, and Z directions were recorded using a Kistler charge amplifier 5070A (Winterthur, Switzerland). A data acquisition system Kistler 5697A2 (Winterthur, Switzerland) and a computer executing the DynoWare software completed the acquisition chain. The sampling frequency was set at 40 kHz, and no filter was applied to the data. The clamping of the parts left visible marks on their cylinders without inducing cracks. Indeed, the binder weight percentage was high enough to allow the part to be deformed without breaking.

The surface topography was evaluated using a DH-6 roughness measurement instrument from Diavite (Bülach, Switzerland). The resulting arithmetic and total roughness (Ra and Rt, respectively) were computed. A qualitative evaluation of the surface topography was also performed using a digital microscope AM7013MZT from Dino-lite (Torrance, CA, USA). The images were acquired using the DinoCapture software version 2.0 and allowed the identification of the generation of material pull-out.

Each selected cutting condition was tested with three different repetitions. During each repetition, three passes were realised. The surface topography was evaluated after the third pass of each repetition while the cutting forces were recorded continuously for each individual pass. In total, 287 tests of three passes were conducted in this study.

The ceramic oxide composing the feedstock was very abrasive and can lead to accelerated wear of the cutting tool. As a consequence, the wear of each tool was monitored after

each pass using the digital microscope AM7013MZT from Dino-lite (Torrance, CA, USA). The presence of uniform or localised wear was assessed using the ISO 8688-2 criteria. No significant flank wear was observed during the tests. This ensured there was no influence of tool wear on the results.

2.3. Tool–Material Couple Standard Application

The tool–material couple standard [23] was used to organise the experiments. The qualification test, determination of $v_{c,min}$ and the range h_{min}–h_{max} were performed. However, the other tests (determination of limiting data ($A_{D,max}$, and Q_{max}), wear tests, and the determination of auxiliary parameters) were not conducted since this paper aims to find the operating condition for the finishing of parts. Indeed, the goal of this kind of operation is to obtain the required surface topography and tolerances. In this framework, $A_{D,max}$ and Q_{max} are of little interest. The wear tests were not followed as in the standard, but the wear of the tool was qualitatively monitored.

2.3.1. Starting Cutting Parameters

Since the selected tools were not directly dedicated to the material milled in this article, no data was available in the supplier catalogues. For each tool, several tests were conducted before beginning the experiments to find a suitable starting cutting speed. Variations of the spindle speed from 3500 rpm to 22,000 rpm by steps of 3500 rpm were conducted (resulting in cutting speed from 66 m/min to 415 m/min). The other cutting parameters a_e, a_p and f_z were set at 0.5 mm, 3 mm and 0.03 mm/tooth, respectively. The criteria to select the cutting speed were: the repeatability of the cutting forces and a surface topography below 1.6 µm Ra without pull-out. Table 2 gives the starting cutting parameters used for each tool.

Table 2. Starting parameters for each tool.

Tool	v_c (m/min)	f_z (mm/tooth)	a_p (mm)	a_e (mm)
Thermoplastics	383			
Composites	324	0.030	3	0.5
Universal	270			

2.3.2. Qualification Test

The qualification test consisted of using the starting conditions and modifying them slightly (between 15% and 20% for this paper) to check if the result of the cutting operation was still acceptable. Table 3 gives the experimental plan that was followed for this test. As for the other tests, each set of parameters was tested with three repetitions, each made of three passes.

Table 3. Experimental plan of the qualification test.

Tool	v_c (m/min)	f_z (mm/tooth)	a_p (mm)	a_e (mm)
Thermoplastics	383	0.030	3	0.5
	443	0.030	3	0.5
	306	0.030	3	0.5
	383	0.036	3	0.5
	383	0.024	3	0.5
	383	0.030	3.6	0.5
	383	0.030	2.4	0.5
	383	0.030	3	0.6
	383	0.030	3	0.4

Table 3. *Cont.*

Tool	v_c (m/min)	f_z (mm/tooth)	a_p (mm)	a_e (mm)
Composites	324	0.030	3	0.5
	389	0.030	3	0.5
	259	0.030	3	0.5
	324	0.036	3	0.5
	324	0.024	3	0.5
	324	0.030	3.6	0.5
	324	0.030	2.4	0.5
	324	0.030	3	0.6
	324	0.030	3	0.4
	324	0.030	3	0.5
Universal	270	0.030	3	0.5
	309	0.030	3	0.5
	228	0.030	3	0.5
	270	0.036	3	0.5
	270	0.024	3	0.5
	270	0.030	3.6	0.5
	270	0.030	2.4	0.5
	270	0.030	3	0.6
	270	0.030	3	0.4

2.3.3. Minimal Cutting Speed

The determination of the minimal cutting speed $v_{c,min}$ required varying the cutting speed while keeping the other parameters (f_z, a_p and a_e) constant. In this paper, the choice was made to scan most of the possible range of the spindle speed (from 3500 rpm to 22,000 rpm). Table 4 gives the different spindle and cutting speeds considered for the determination of $v_{c,min}$. The same range was considered for all the tools.

Table 4. Range of N (in rpm) and v_c (in m/min) considered for the determination of $v_{c,min}$.

N (rpm)	v_c (m/min)
3500	66
7000	132
11,000	207
14,300	270
16,400	309
17,200	324
18,600	351
20,300	383
22,000	415

2.3.4. Mean Chip Thickness Range

Finally, the determination of the mean chip thickness (h_m) range was explored by modifying the feed per tooth (f_z) while keeping the other parameters (v_c, a_p and a_e) constant. The range of variation of f_z, as well as the resulting chip thickness h_m, is given in Table 5.

Table 5. Range of f_z (in mm/tooth) and h_m (in mm) considered for the determination of the mean chip thickness range.

f_z (mm/tooth)	h_m (mm)
0.003	0.001
0.005	0.003
0.010	0.006
0.015	0.008
0.021	0.012
0.030	0.017
0.039	0.022
0.051	0.028
0.066	0.036

2.4. Computation of the Specific Cutting Energy

All the conducted tests required the computation of the specific cutting energy. This specific energy is the ratio between the cutting power and the material removal rate. As the cutting forces were low during the tests (mainly lower than 20 N), it was not possible to record the cutting power during the experiments with an acceptable signal-to-noise ratio. Moreover, the reference frame of the dynamometer was not the same as the tool. Consequently, the total cutting forces along the X, Y, and Z axis of the dynamometer were used to determine the specific cutting energy instead of using the results of the feed and tangential cutting forces. Indeed, there is a proportional link between the tangential component of the force and its radial and axial components, as demonstrated in the recent paper of Demarbaix et al. [22]. The RMS value of the total resulting force for each pass was then used as a representative value.

The total resulting force (in N) was computed as follows:

$$F_{tot} = \sqrt{F_x^2 + F_y^2 + F_z^2} \tag{1}$$

Finally, as finishing operations were conducted by milling straight shoulders, the radial depth of cut was always less than half of the tool diameter. The mean chip thickness h_m (in mm) can then be computed as:

$$h_m = 2 \cdot f_z \cdot \sqrt{(\frac{a_e}{D}) \cdot (1 - \frac{a_e}{D})} \tag{2}$$

The resulting specific cutting energy (in $\frac{\text{W·min}}{\text{cm}^3}$) can be expressed as:

$$W_c = \beta \cdot \frac{F_{tot}}{60 \cdot a_p \cdot h_m} \tag{3}$$

where β is a real number. For the sake of simplicity, the right-hand side of the equation divided by β will be called specific cutting energy in the present paper since it is directly proportional to it.

3. Results and Discussion

3.1. Qualification Test

For the three tools, the results of the surface topography and specific cutting energy for the qualification test are given in Figures 6–15. In Figures 6, 10, and 13, two red lines give the domain of the 1.6 µm Ra class (from 0.8 µm to 1.6 µm). Each point of data was given $\pm\sigma$ error bars. Indeed, each point on the graph shows the mean value of three measurements carried out with the same cutting parameters. The considered cutting parameters are given with v_c (m/min), f_z (mm/tooth), a_p (mm), and a_e (mm). Figures 8, 9, 12, and 15 show qualitatively the surface topography generated with the milling operations for the qualification point of each tool. In these Figures, only the vertical surface (according to the X and Z axes) generated by the tool is shown. Indeed, in a finishing context, the horizontal surface (according to the X and Y axes) will not exist.

For the thermoplastic tool (Figure 6), all the results are below the 0.8 µm threshold bar. Indeed, all the results belong to the 0.8 µm instead of the 1.6 µm Ra class. The results range from 0.48 µm to 0.71 µm. The repeatability of results is good, with a dispersion of about 15% around the mean for all experiments. In terms of specific cutting energy (Figure 7), the results vary between 2.67 W·min/cm^3 and 6.98 W·min/cm^3. There are variations up to 100% between the different cutting conditions. The high variation of results can be explained by the relatively high variation in cutting conditions imposed on the tool. Indeed, v_c (m/min), f_z (mm/tooth), a_p (mm), and a_e (mm) were modified by 20%. Even though there were significant variations between the different cutting conditions, the repeatability of results for a given set of cutting parameters was very good (about 4% of the mean).

All the different tests produced a surface topography without material pull-out, as shown in Figure 8 for the parameters v_c = 383 m/min, f_z = 0.030 mm/tooth, a_p = 3 mm, and

a_e = 0.5 mm. The milled surface is shown with the red arrow. As depicted in the picture, the surface topography was shiny and without pull-out as required.

However, there is a zone of approximatively 0.85 mm where the material was not completely cut (see the blue arrow in Figure 8). Figure 9 depicts a side view of the milled straight shoulder. The uncut material is shown again with a blue arrow. All passes performed with the tool dedicated to thermoplastics exhibited the same uncut zone. This, therefore, has to be taken into account when performing the milling of parts. Indeed, by shifting the tool further down, this uncut material can be removed. Consequently, as the goals to achieve were ensuring repeatable results while respecting a Ra class of 1.6 µm without material pull-out, the selected cutting conditions were validated.

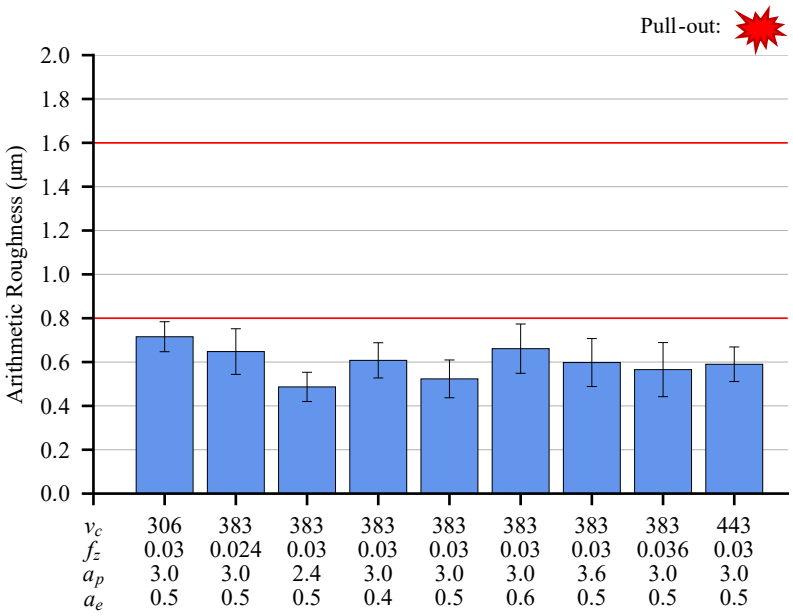

Figure 6. Qualification test of the thermoplastic tool, the evolution of Ra (µm) for different v_c (m/min), f_z (mm/tooth), a_p (mm), and a_e (mm). No material pull-out was observed.

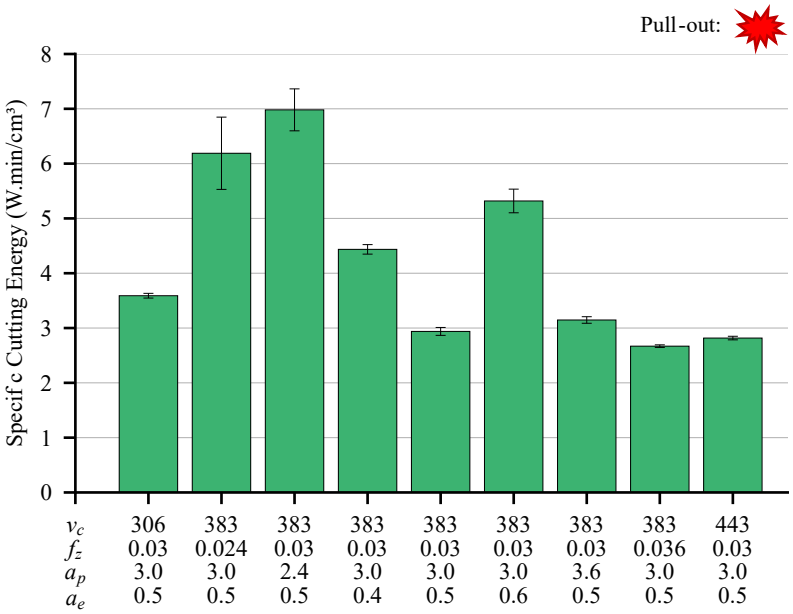

Figure 7. Qualification test of the thermoplastic tool, evolution of W_c (W·min/cm^3) for different v_c (m/min), f_z (mm/tooth), a_p (mm), and a_e (mm). No material pull-out was observed.

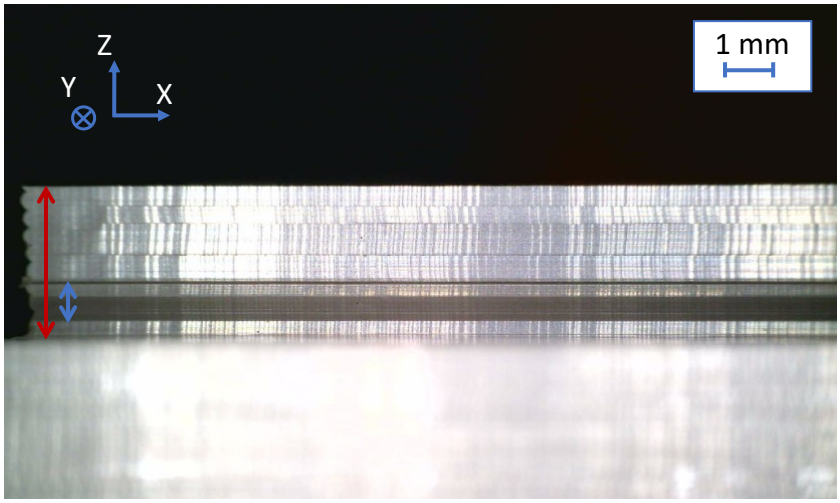

Figure 8. Surface topography of the qualification point for the tool dedicated to thermoplastics, v_c = 383 m/min, f_z = 0.030 mm/tooth, a_p = 3 mm, and a_e = 0.5 mm. No material pull-out was observed.

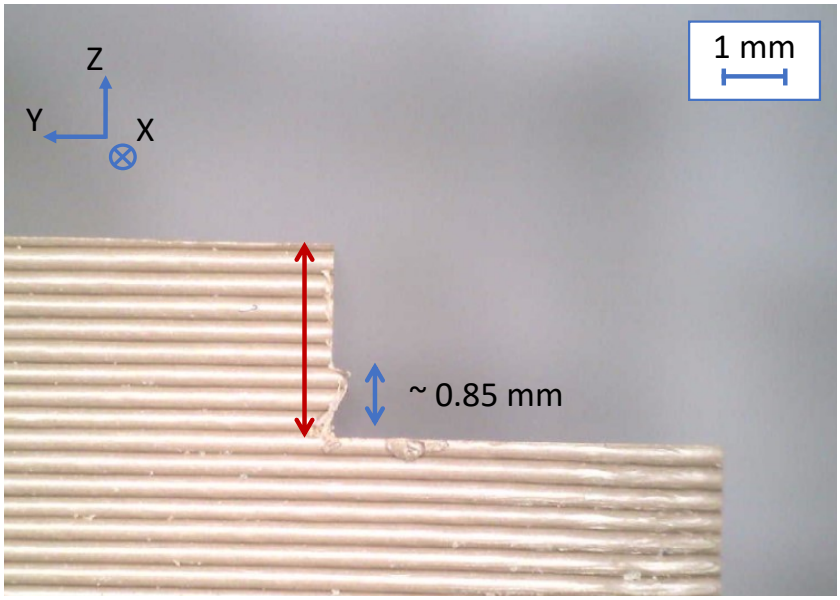

Figure 9. Side view of the milled straight shoulder for the thermoplastic tool.

The qualification test of the composite tool is depicted in Figure 10 for the surface topography results. As can be seen in the graph, all the results of Ra are strictly inside the 1.6 µm Ra class delimited by the red lines. The results go from 0.88 µm to 1.22 µm with a dispersion for each condition representing, on average, 10% of the mean value. As shown in Figure 11, the specific cutting energy ranges from 1.75 W·min/cm^3 and 2.96 W·min/cm^3. The variations between different cutting conditions reached a maximum of 70% and were lower than for the thermoplastic tool. On average, the dispersion of measurements for a given set of cutting parameters reached 5%. This means again that repeatable results were obtained.

All the different tests produced a smooth surface topography without material pull-out, as depicted in Figure 12, for v_c = 324 m/min, f_z = 0.030 mm/tooth, a_p = 3 mm, and a_e = 0.5 mm. Again, the milled surface is shown with the red arrow. As depicted in the picture, there was an absence of pull-out, but there was a shiny finish. In contrast with the tool dedicated to the thermoplastics, all the desired material to remove was cut. Again, the working point selected was validated.

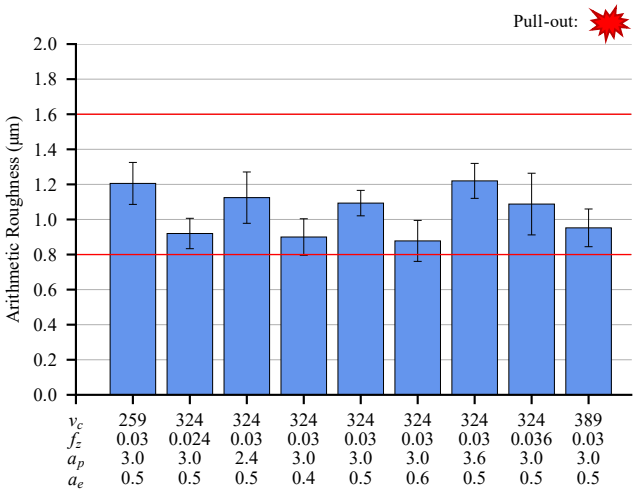

Figure 10. Qualification test of the composite tool, the evolution of Ra (µm) for different v_c (m/min), f_z (mm/tooth), a_p (mm), and a_e (mm). No material pull-out was observed.

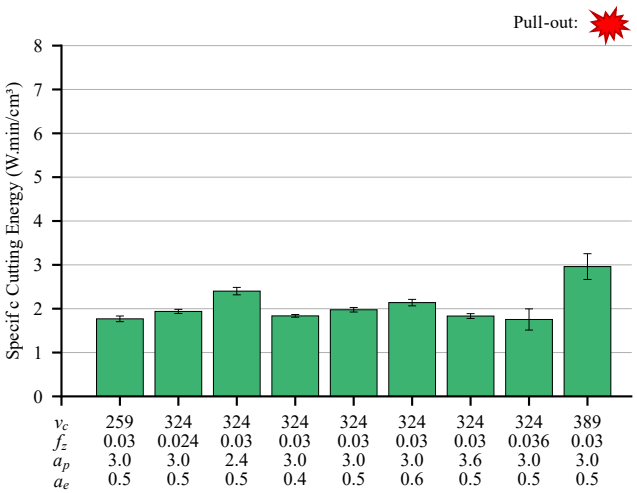

Figure 11. Qualification test of the composite tool, the evolution of W_c (W·min/cm^3) for different v_c (m/min), f_z (mm/tooth), a_p (mm), and a_e (mm). No material pull-out was observed.

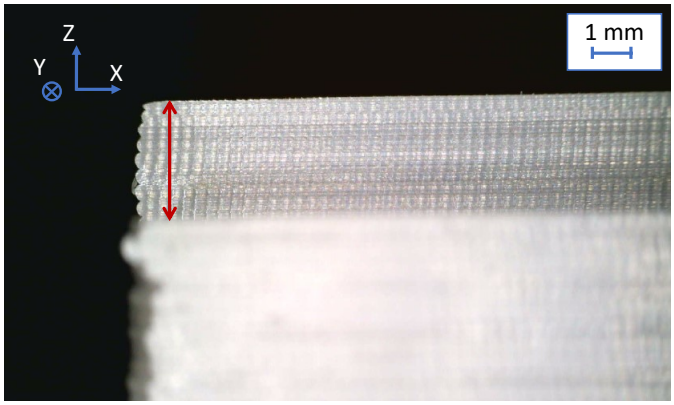

Figure 12. Surface topography of the qualification point for the tool dedicated to composites, v_c = 324 m/min, f_z = 0.030 mm/tooth, a_p = 3 mm, and a_e = 0.5 mm. No material pull-out was observed.

The working point of the universal tool was evaluated as exhibited in Figure 13. For this tool, the results of surface topography were between 0.68 µm and 0.86 µm. The dispersion of each cutting condition represents, as for the other tools, about 13% of the measured Ra. Some of the results were included in the 1.6 µm Ra class, while others were

inside the 0.8 µm Ra class. The specific cutting energy of the universal tool, as depicted in Figure 14, went from 3.49 W·min/cm^3 to 5.35 W·min/cm^3. As for the thermoplastic tool, high variations were measured for different cutting conditions. Again, their origin probably comes from the high variations imposed on the cutting parameters. However, the repeatability of the measurements was the best among the three tools, with variations of only 1% around the mean value for a given set of cutting parameters.

The surface topography of the qualification point for the universal tool is depicted in Figure 15 (v_c = 270 m/min, f_z = 0.030 mm/tooth, a_p = 3 mm, and a_e = 0.5 mm). As can be seen in the Figure, material pull-out occurred during the pass (circled in yellow). It should be noted that only a few tests were free from these defects. The absence of material pull-out was a requirement for the tool to be selected. This means that the universal tool cannot be used for the finishing of green ceramics obtained using the PAM process. Even with this information, the other tests of the method were performed.

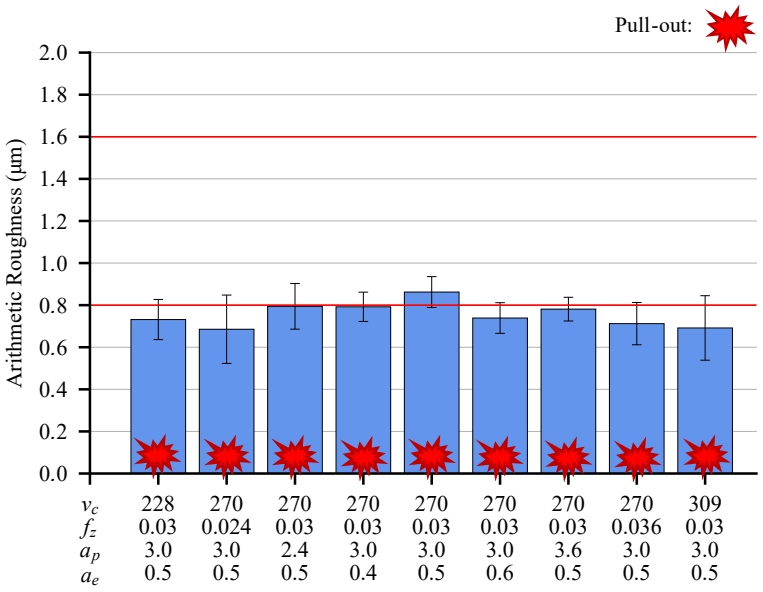

Figure 13. Qualification test of the universal tool, the evolution of Ra (µm) for different v_c (m/min), f_z (mm/tooth), a_p (mm), and a_e (mm).

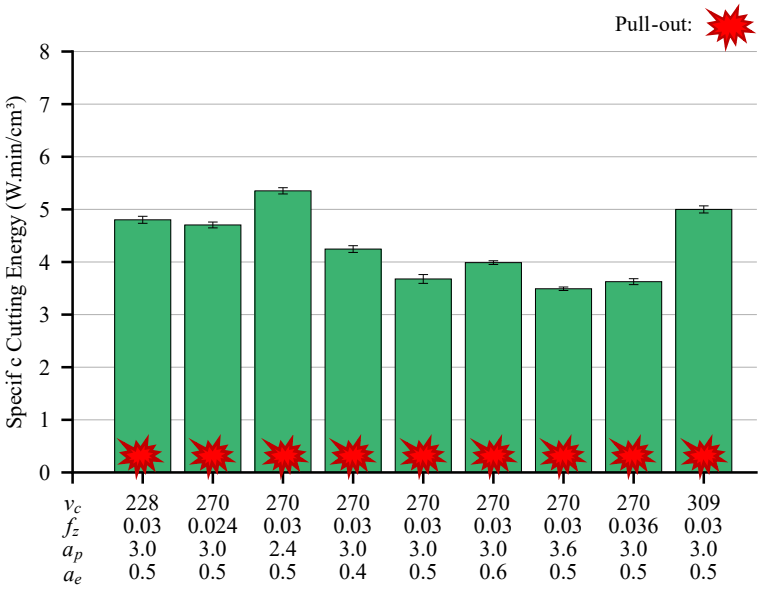

Figure 14. Qualification test of the universal tool, the evolution of W_c (W·min/cm^3) for different v_c (m/min), f_z (mm/tooth), a_p (mm), and a_e (mm).

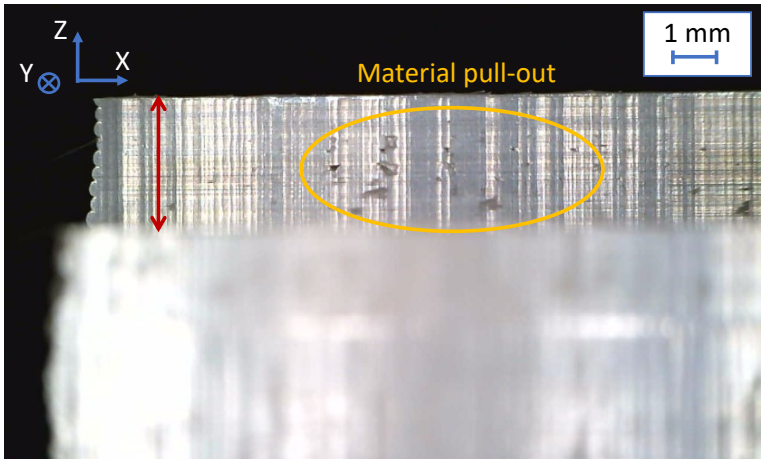

Figure 15. Surface topography of the qualification point for the universal tool, v_c = 270 m/min, f_z = 0.030 mm/tooth, a_p = 3 mm, and a_e = 0.5 mm.

The reference points of the thermoplastic and composite tools were validated since they allowed a smooth surface finish to be obtained while respecting a Ra class of 1.6 µm and producing repeatable results. Conversely, even though the universal tool exhibited the best repeatability results of specific cutting energy, it produced material pull-out for almost all tested cutting conditions. Consequently, the universal tool cannot be qualified for the green zirconia used in this study.

3.2. Determination of the Minimal Cutting Speed

Figure 16 give the arithmetic roughness for different values of v_c, for the thermoplastic tool. All the other cutting parameters were constant (f_z = 0.030 mm/tooth, a_p = 3 mm, and a_e = 0.5 mm). Two red lines delimit the domain of the 1.6 µm Ra class. The specific cutting energy is also depicted in Figure 17 for the same tool. As before, each point of measurement is the average of three measurements and is depicted on the graph with a $\pm\sigma$ error bar. Figures 18 and 19 give the arithmetic roughness and specific cutting energy for the composite tool, respectively. So do Figures 20 and 21 for the universal tool.

The tool–material couple standard [23] gives the expected trend of the specific cutting energy for the minimal cutting speed determination. By increasing the cutting speed and keeping all other parameters constant, the specific cutting energy should exhibit a sudden drop and should then continue to decrease at a lower rate. In some cases, the specific energy does not follow this trend and requires taking into account other parameters, such as the surface topography.

Figure 16 gives the achieved Ra for the thermoplastic tool. As depicted on the graph, the general trend decreased as required by the tool–material couple standard [23]. All the results were below the 1.6 µm threshold and even below the 0.8 µm threshold when the cutting speed was higher than 309 m/min. From 309 m/min to 415 m/min, the results of Ra tended to reach a plateau. However, at 309 m/min, the repeatability was lower than for higher cutting speeds. Indeed, at this speed, the dispersion of measurements achieved 31% around the mean value while it was only 16% on average from 324 m/min to 383 m/min. All the tested cutting speeds produced a smooth surface topography without pull-out as required.

The specific cutting energy did not follow the same trend. Indeed, as depicted in Figure 17, the cutting energy varied between 1.88 W·min/cm^3 and 4.04 W·min/cm^3 but without a globally decreasing trend. Consequently, the specific cutting energy could not be used as the only indicator to determine the minimal cutting speed. As a consequence, the minimal cutting speed was selected thanks to the arithmetic roughness evolution. The value selected was 324 m/min since, after this speed, the dispersion was lower than for the 309 m/min cutting speed.

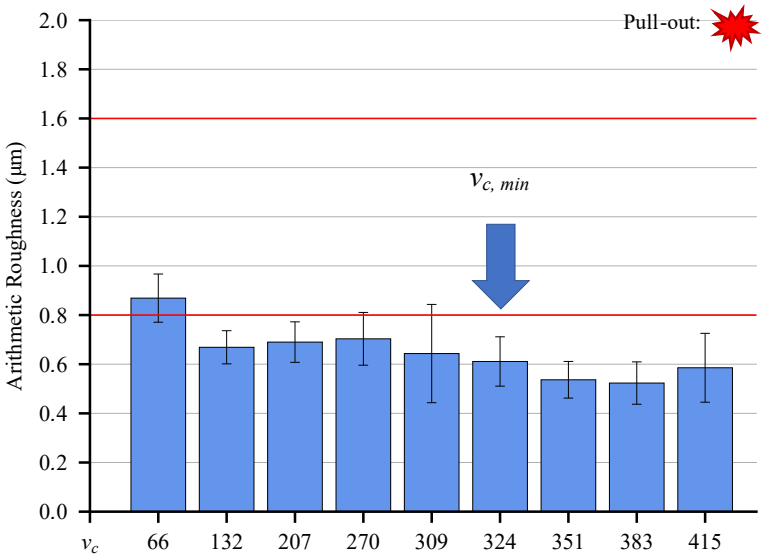

Figure 16. Determination of the minimal cutting speed of the thermoplastic tool, evolution of the arithmetic roughness (µm) for different v_c (m/min) with f_z = 0.030 mm/tooth, a_p = 3 mm, and a_e = 0.5 mm. No material pull-out was observed.

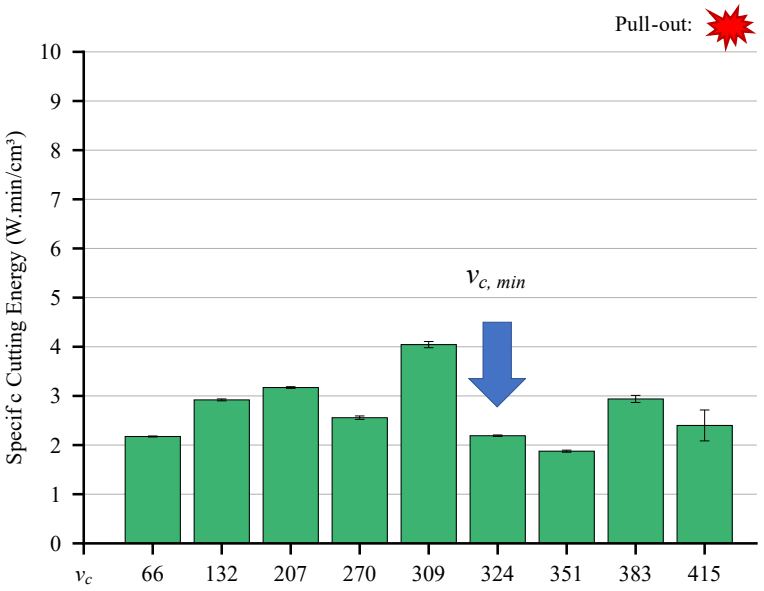

Figure 17. Determination of the minimal cutting speed of the thermoplastic tool, the evolution of the specific cutting energy (W·min/cm^3) for different v_c (m/min) with f_z = 0.030 mm/tooth, a_p = 3 mm, and a_e = 0.5 mm. No material pull-out was observed.

The arithmetic roughness of the composite tool for different cutting speeds is given in Figure 18. As depicted in the graph, there is a decreasing trend, as expected. All the values were within the 1.6 µm Ra class. After 351 m/min, the results stabilize and achieve a plateau. The dispersion of measurements does not decrease dramatically when the cutting speed increases. Indeed, it represents, on average, 9.5% of the mean value. The machined surface exhibited pull-out only for the 66 m/min cutting speed. All the other points produced a smooth surface topography.

As for the thermoplastic tool, the specific cutting energy did not show a decreasing trend when the cutting speed increased, as presented in Figure 19. Again, the specific cutting energy could not be used alone to determine the minimal cutting speed. Consequently, 351 m/min was selected as the minimal cutting speed according to the arithmetic roughness evolution.

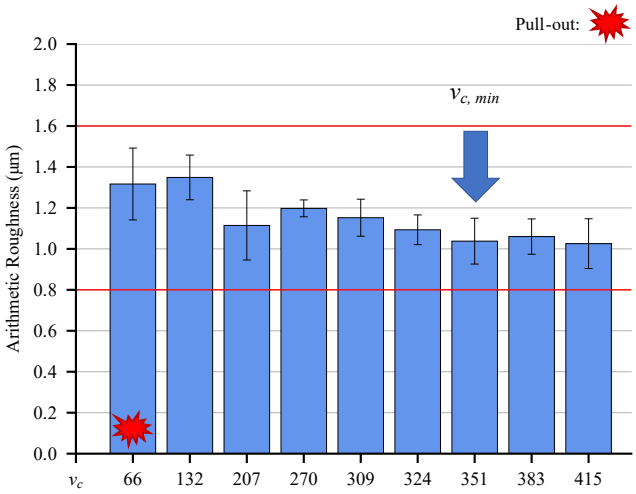

Figure 18. Determination of the minimal cutting speed of the composite tool, evolution of the arithmetic roughness (µm) for different v_c (m/min) with f_z = 0.030 mm/tooth, a_p = 3 mm, and a_e = 0.5 mm.

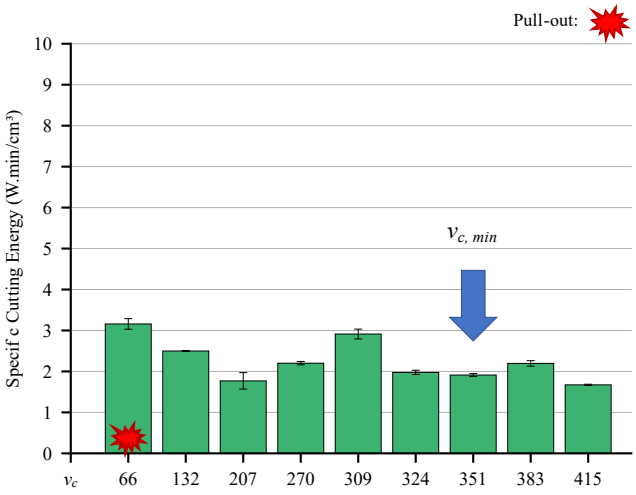

Figure 19. Determination of the minimal cutting speed of the composite tool, evolution of the specific cutting energy (W·min/cm^3) for different v_c (m/min) with f_z = 0.030 mm/tooth, a_p = 3 mm, and a_e = 0.5 mm.

The evolution of the arithmetic roughness of the universal tool for different cutting speeds is depicted in Figure 20. As can be seen in the graph, high variations of results were recorded compared to the two other tools. Surprisingly, the results of arithmetic roughness were better (<0.8 µm) for the lowest cutting speeds (66 m/min and 132 m/min). However, the repeatability of results was lower than for the other tested tools. Indeed, for each considered cutting speed, one or two tests produced pull-out. As a consequence, the universal tool could not be used with this material. Indeed, the repeatability of results was one of the required conditions for selecting one of the tools.

The specific cutting energy showed the same trend as the arithmetic roughness. High variations were recorded across the domain of the tested cutting speeds. As for the surface topography, the lowest tested cutting speeds exhibited the best results of specific energy. Difficulty in evacuating the chips may explain the higher specific cutting energy at higher cutting speeds. However, with the evolution of arithmetic roughness, a minimal cutting speed of 351 m/min can be selected. Indeed, after 324 m/min, the arithmetic roughness dramatically decreased, as well as the measurement dispersion. For the same cutting speed as the reference point (v_c = 270 m/min), the Ra results of Figure 20 are higher. Nevertheless, the results of the qualification test are included within the error bars of

Figure 20. The selected minimal cutting speed is also higher than the cutting speed of the reference point. This is the result of the standard method, which first tests a reference point before selecting the minimal cutting speed. However, even with a higher cutting speed for the qualification test, the universal tool produced a surface topography with material pull-out. The conclusions are then the same.

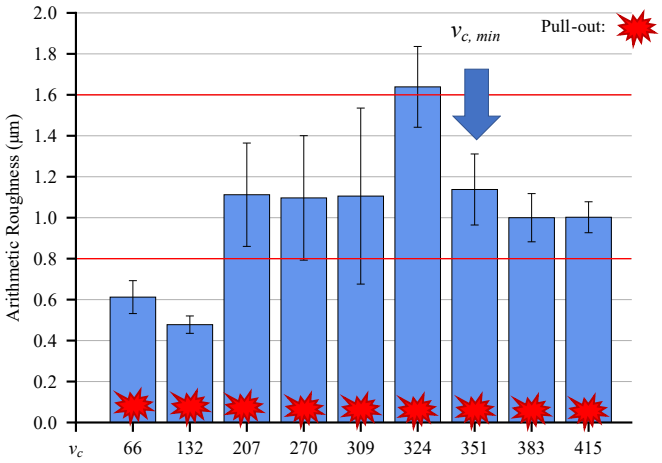

Figure 20. Determination of the minimal cutting speed of the universal tool, the evolution of the arithmetic roughness (µm) for different v_c (m/min) with f_z = 0.030 mm/tooth, a_p = 3 mm, and a_e = 0.5 mm.

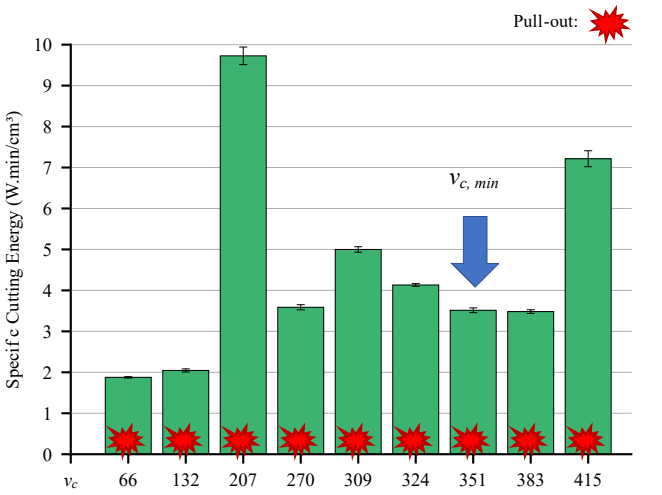

Figure 21. Determination of the minimal cutting speed of the universal tool, the evolution of the specific cutting energy (W·min/cm^3) for different v_c (m/min) with f_z = 0.030 mm/tooth, a_p = 3 mm, and a_e = 0.5 mm.

As depicted in Figures 16–21, and except for the universal tool, the arithmetic roughness showed the expected decreasing trend when the cutting speed increased. However, the specific cutting energy did not exhibit the same behaviour. The minimal cutting speed was, therefore, selected solely based on the arithmetic roughness. The composite tool allowed results within the 1.6 µm Ra class, while the thermoplastic tool reached better results within the 0.8 µm Ra class. Repeatable results and a surface without material pull-out were obtained for both tools. Conversely, the universal tool exhibited higher variations of results, as well as material pull-out on each of the considered cutting conditions. For the specific energy, again, the thermoplastic and composite tools produced repeatable results while the universal tool did not. As a result, the universal tool cannot be selected to realize finishing operations on zirconia green ceramics, while the thermoplastic and composite tools can be good candidates.

3.3. Determination of the Minimal and Maximal Chip Thickness

Figures 22–24 show, for the three selected tools, the evolution of W_c (W·min/cm^3, in green) and Ra (µm, in blue) for different average chip thicknesses h_m (mm). Each point of measurement was given a $\pm\sigma$ error bar showing the measurement dispersion.

As described in the tool–material couple standard [23] , by varying the chip thickness while keeping all other parameters constant, the specific energy should exhibit a decreasing trend with a sudden drop. The chip thickness at this drop is the lower limit of chip thickness (h_{min}). After this value of h_m, the specific energy should continue to decrease at a slower pace. The determination of the high limit (h_{max}) of the chip thickness requires taking into account the surface topography and the apparition of interfering phenomena such as material pull-out or exceeding the maximum allowed arithmetic roughness. Indeed, when the chip thickness increases, the surface topography degrades progressively and can result in the apparition of material pull-out.

The evolution of the specific cutting energy and arithmetic roughness of the thermoplastic tool is given for different values of h_m (mm) in Figure 22. For these tests, the v_c chosen was 324 m/min (equal to $v_{c,min}$), while a_p and a_e were set at 3 mm and 0.5 mm, respectively. As depicted in the graph, the specific cutting energy decreased when the average chip thickness increased while the arithmetic roughness increased. At 0.048 mm of h_m, the Ra was still below the 1.6 µm threshold, but pull-out appeared in all tests, and the dispersion of measurements increased dramatically. The previously tested value of h_m (0.036 mm) was then selected as the high limit of chip thickness. The specific cutting energy showed a sudden decrease for an average chip thickness of 0.003 mm. This value was then selected as the low limit of chip thickness. For the thermoplastic tool, the chip thickness range ranged between 0.003 mm and 0.036 mm, as depicted with a grey background in Figure 22. These two values of h_m corresponded to feed rates (v_f) of 263 mm/min and 3401 mm/min, respectively.

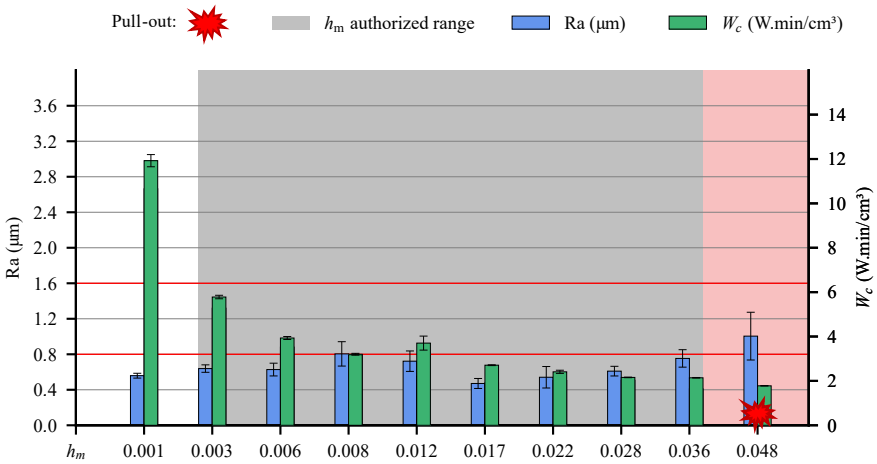

Figure 22. Evolution of the specific cutting energy (W·min/cm^3) and Ra (µm) of the thermoplastic tool for different h_m (mm) with v_c = 324 m/min, a_p = 3 mm, and a_e = 0.5 mm.

Figure 23 allows the determination of the low and high limits of chip thickness for the composite tool. As for the thermoplastic tool, v_c was chosen equal to $v_{c,min}$ (351 m/min), while a_p and a_e were set at 3 mm and 0.5 mm, respectively. As expected, W_c and its measurement dispersion decreased when h_m increased. In contrast with the thermoplastic tool, the arithmetic roughness achieved values higher than the 1.6 µm threshold for low values of h_m. The first chip thickness leading to a Ra below the threshold was 0.003 mm. As for the thermoplastic tool, this value was selected as the low limit for h_m. The arithmetic roughness also allowed the selection of the high value of h_m. Indeed, the value of Ra and its dispersion were higher than the 1.6 µm threshold for 0.028 mm of h_m. As a consequence, 0.022 mm of h_m was selected as the high value. It should be noted that no pull-out was generated for all the tested values of h_m. The range of h_m ranges then from 0.003 mm to

0.022 mm, as shown in grey in Figure 23. The corresponding feed rates were 957 mm/min and 9430 mm/min.

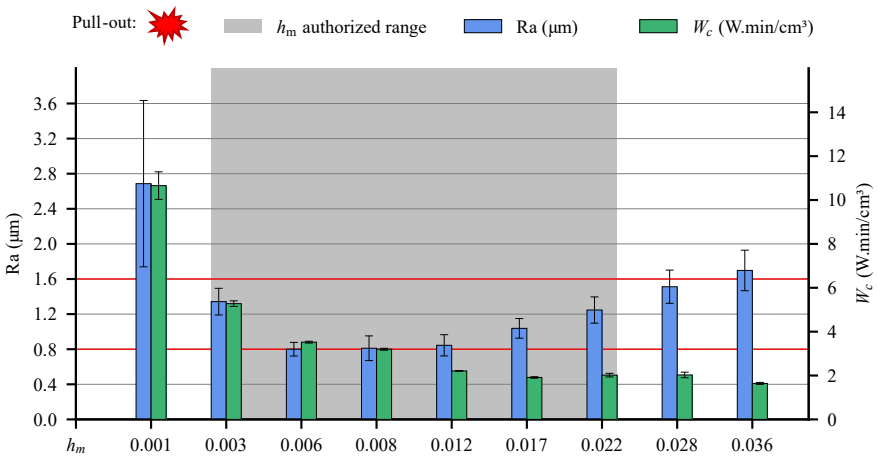

Figure 23. Evolution of the specific cutting energy (W·min/cm^3) and Ra (µm) of the composite tool for different h_m (mm) with v_c = 351 m/min, a_p = 3 mm and a_e = 0.5 mm No material pull-out was observed.

The high and low limits of h_m for the universal tool can be obtained from Figure 24. The cutting speed v_c selected was the same as the qualification point (v_c = 270 m/min), while a_p and a_e were set at 3 mm and 0.5 mm, respectively. As for the two other tools, the specific cutting energy showed a decreasing trend, while the surface topography deteriorated when h_m increased. At an average chip thickness of 0.017 mm, there was a sudden drop in specific cutting energy. All the results of Ra were below the 1.6 µm threshold. Nevertheless, pull-out was produced for all the tested h_m, except for the values of 0.048 mm and 0.062 mm. These two values can be taken as low and high values of chip thickness as shown in grey in Figure 24. These correspond to feed rates of 3689 mm/min and 4779 mm/min. Again, the universal tool shows a lower potential for being used to mill green zirconia parts since it exhibits the lowest range of eligible h_m compared to the thermoplastic and composite tools.

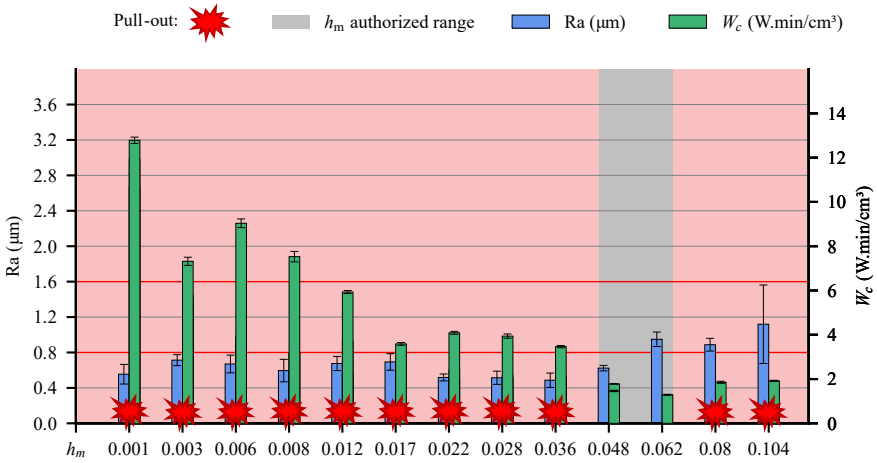

Figure 24. Evolution of the specific cutting energy (W·min/cm^3) and Ra (µm) of the universal tool for different h_m (mm) with v_c = 270 m/min, a_p = 3 mm and a_e = 0.5 mm

3.4. Tool Selection

Only a few of the tests carried out with the universal tool were without material pull-out and with repeatable results. This complicated the use of the tool since only a few cutting conditions could be used to obtain the desired surface topography. As a consequence, this tool could not be used to finish the green ceramics obtained using the PAM process.

The tools dedicated to the machining of composites and thermoplastics allowed the desired surface topography in terms of arithmetic roughness and the absence of material pull-out to be obtained. Their minimal and maximal average chip thickness range allowed their use with different feeds per tooth to be foreseen. However, the maximal average chip thickness of the thermoplastic tool was higher than for the composite tool (0.036 mm vs. 0.022 mm) while maintaining the arithmetic roughness at a lower level. Indeed, at an average chip thickness of 0.036 mm, the tool dedicated to the thermoplastics achieved a Ra of 0.75 µm on average, while the tool for composites reached a Ra of 1.25 µm for an average chip thickness of 0.022 mm.

Nevertheless, the material removal rate of the thermoplastic tool is two times lower than for the composite tool at the maximal average thickness (5.06 cm^3/min vs. 10.96 cm^3/min). Indeed, the composite tool has ten teeth, while the thermoplastic tool has only three. In terms of cost, the thermoplastic tool is about four times more affordable than the composite tool.

The lower cost, achievable Ra, absence of pull-out and larger chip thickness range of the thermoplastic tool make it the best compromise to ensure the finishing of additively manufactured green zirconia. Nevertheless, the uncut zone generated must be taken into account when planning the milling operations.

Table 6 gives the main cutting parameter limits of the thermoplastic and composite tools. Both can be used for the low-cost finishing of additively manufactured zirconia green parts. Though, the thermoplastic tool appears to be the best compromise between price and performance.

Table 6. Main cutting parameter limits of the thermoplastic and composite tools.

	Thermoplastic Tool	**Composite Tool**
$v_{c,min}$ (m/min)	324	351
$h_{m,min}$ (mm)/$f_{z,min}$ (mm)	0.003/0.005	0.003 /0.005
$h_{m,max}$ (mm)/$f_{z,max}$ (mm)	0.036/0.066	0.022 /0.039

4. Conclusions

Even though the PAM process is bringing new possibilities in terms of feedstock, it still suffers from rough surface topography and large geometrical and dimensional tolerances. Finishing operations are then required to obtain a part with a smooth surface and tight tolerances. Three standard tools (dedicated to thermoplastics, composites, and a universal tool) were tested according to the tool–material couple standard. The allowed cutting conditions were determined with the goal of ensuring the finishing operation (repeatable results of Ra $<$ 1.6 µm and absence of material pull-out) of green zirconia parts obtained by the PAM process at a lower cost.

The main findings are the following:

- Even though the tool–material couple standard is dedicated to ductile materials, its systematic approach and objective methodology allow us to determine experimentally the cutting parameters in additively manufactured zirconia. This methodology can be used to determine the finishing cutting parameters of other additively manufactured materials using a thermoplastic binder system. Indeed, a wide variety of materials (Ti6Al4V, AISI 316L, Al_2O_3, etc.) are already available as injection moulding feedstocks using a thermoplastic binder and can be shaped with the PAM process, as the green zirconia used in this study.
- The thermoplastic tool is the most affordable while exhibiting the largest chip thickness range and the best achievable surface topography (Ra $<$ 0.8 µm).
- The tool dedicated to composites is four times more expensive than the thermoplastic tool. However, it cannot achieve a surface topography as low as the thermoplastic tool (minimal Ra standing at 0.8 µm while the thermoplastic tool can achieve a minimal Ra of 0.47 µm).
- Repeatable results of surface topography and specific cutting energy were obtained for the thermoplastic and composite tools.

- Only a few tests were without material pull-out for the universal tool, while a large dispersion of measurements was observed. This tool cannot be selected since the absence of material pull-out was a requirement, as well as repeatable results. The other tools only exhibited material pull-out at the extreme limits of their usage domain (maximal average chip thickness, for example).

The recommended cutting conditions for the finishing of AM green zirconia parts using the thermoplastic tool are $v_{c,min} > 324$ m/min, f_z between 0.005 mm/tooth and 0.066 mm/tooth, while the composite tool should be used with $v_{c,min} > 351$ m/min, f_z between 0.005 mm/tooth and 0.039 mm/tooth.

Author Contributions: Conceptualization, F.D., E.R.-L. and L.S.; methodology, L.S.; software, L.S.; validation, F.D., E.R.-L. and L.S.; formal analysis, L.S.; investigation, L.S. and H.D.; resources, F.D., E.R.-L. and J.B.; data curation, L.S. and H.D.; writing—original draft preparation, L.S.; writing—review and editing, F.D., E.R.-L. and L.S.; visualization, L.S.; supervision, F.D. and E.R.-L.; project administration, L.S., F.D. and E.R.-L.; funding acquisition, F.D. and E.R.-L. All authors have read and agreed to the published version of the manuscript.

Funding: This research was funded by the Wallonian regional government thanks to a Win²Wal funding instrument (HyProPAM research project, grant number: 2110084).

Data Availability Statement: The data presented in this study are available on request from the corresponding author.

Acknowledgments: The authors would like to thank the Belgium Ceramic Research Centre (BCRC) for the use of their Pollen AM Series MC printer.

Conflicts of Interest: The authors declare no conflict of interest. The funder had no role in the design of the study; in the collection, analyses, or interpretation of data; in the writing of the manuscript; or in the decision to publish the results.

References

1. Galusek, D.; Ghillányová, K. Ceramic Oxides. In *Ceramics Science and Technology*; Riedel, R., Chen, I.W., Eds.; Wiley-VCH Verlag GmbH & Co. KGaA: Weinheim, Germany, 2014; pp. 1–58. [CrossRef]
2. Altıparmak, S.C.; Yardley, V.A.; Shi, Z.; Lin, J. Extrusion-based additive manufacturing technologies: State of the art and future perspectives. *J. Manuf. Process.* **2022**, *83*, 607–636. [CrossRef]
3. Ferraris, E.; Vleugels, J.; Guo, Y.; Bourell, D.; Kruth, J.P.; Lauwers, B. Shaping of engineering ceramics by electro, chemical and physical processes. *CIRP Ann.-Manuf. Technol.* **2016**, *65*, 761–784. [CrossRef]
4. Demarbaix, A.; Mulliez, M.; Rivière-Lorphèvre, E.; Spitaels, L.; Duterte, C.; Preux, N.; Petit, F.; Ducobu, F. Green Ceramic Machining: Determination of the Recommended Feed Rate for Y-TZP Milling. *J. Compos. Sci.* **2021**, *5*, 231. [CrossRef]
5. Parenti, P.; Cataldo, S.; Grigis, A.; Covelli, M.; Annoni, M. Implementation of hybrid additive manufacturing based on extrusion of feedstock and milling. *Procedia Manuf.* **2019**, *34*, 738–746. [CrossRef]
6. Ferrage, L.; Bertrand, G.; Lenormand, P.; Grossin, D.; Ben-Nissan, B. A review of the additive manufacturing (3DP) of bioceramics: Alumina, zirconia (PSZ) and hydroxyapatite. *J. Aust. Ceram. Soc.* **2017**, *53*, 11–20. [CrossRef]
7. Gonzalez-Gutierrez, J.; Cano, S.; Schuschnigg, S.; Kukla, C.; Sapkota, J.; Holzer, C. Additive manufacturing of metallic and ceramic components by the material extrusion of highly-filled polymers: A review and future perspectives. *Materials* **2018**, *11*, 840. [CrossRef]
8. Krolikowski, M.A.; Krawczyk, M.B. Does Metal Additive Manufacturing in Industry 4.0 Reinforce the Role of Substractive Machining. In *Advances in Manufacturing II*; Trojanowska, J., Ciszak, O., Machado, J.M., Pavlenko, I., Eds.; Springer International Publishing: Cham, Switzerland, 2019; pp. 150–164. [CrossRef]
9. Galante, R.; Figueiredo-Pina, C.G.; Serro, A.P. Additive manufacturing of ceramics for dental applications: A review. *Dent. Mater.* **2019**, *35*, 825–846. [CrossRef]
10. Bourell, D.; Kruth, J.P.; Leu, M.; Levy, G.; Rosen, D.; Beese, A.M.; Clare, A. Materials for additive manufacturing. *CIRP Ann.* **2017**, *66*, 659–681. [CrossRef]
11. Thompson, M.K.; Moroni, G.; Vaneker, T.; Fadel, G.; Campbell, R.I.; Gibson, I.; Bernard, A.; Schulz, J.; Graf, P.; Ahuja, B.; et al. Design for Additive Manufacturing: Trends, opportunities, considerations, and constraints. *CIRP Ann.-Manuf. Technol.* **2016**, *65*, 737–760. [CrossRef]
12. Analysis, S. Ceramics Additive Manufacturing Markets 2017–2028, an Opportunity Analysis and Ten-Year Market Forecast, Technical Report. 2018. Available online: https://www.smartechanalysis.com/reports/ceramics-additive-manufacturing-markets-2017-2028/ (accessed on 6 March 2023).

13. Moinard, D.; Rigollet, C. Procédés de Frittage PIM. Techniques de l'Ingénieur. M3320 v1. 2011. Available online: https://www.techniques-ingenieur.fr/base-documentaire/materiaux-th11/ceramiques-proprietes-et-elaboration-42578210/procedes-de-frittage-pim-m3320/ (accessed on 6 March 2023).
14. Rane, K.; Strano, M. A comprehensive review of extrusion-based additive manufacturing processes for rapid production of metallic and ceramic parts. In *Advances in Manufacturing*; Shanghai University: Shanghai, China, 2019; Volume 7, pp. 155–173. [CrossRef]
15. Turner, B.N.; Gold, S.A. A review of melt extrusion additive manufacturing processes: II. Materials, dimensional accuracy, and surface roughness. *Rapid Prototyp. J.* **2015**, *21*, 250–261. [CrossRef]
16. Kumbhar, N.N.; Mulay, A.V. Post Processing Methods used to Improve Surface Finish of Products which are Manufactured by Additive Manufacturing Technologies: A Review. *J. Inst. Eng. India Ser. C* **2018**, *99*, 481–487. [CrossRef]
17. Hung, W. Post-Processing of Additively Manufactured Metal Parts. In *Additive Manufacturing Processes*; Bourell, D.L., Frazier, W., Kuhn, H., Seifi, M., Eds.; ASM International: Geauga, OH, USA, 2020; pp. 298–315.
18. Spitaels, L.; Rivière-Lorphèvre, E.; Díaz, M.C.; Duquesnoy, J.; Ducobu, F. Surface finishing of EBM parts by (electro-)chemical etching. *Procedia CIRP* **2022**, *108*, 112–117. [CrossRef]
19. Uçak, N.; Çiçek, A.; Aslantas, K. Machinability of 3D printed metallic materials fabricated by selective laser melting and electron beam melting: A review. *J. Manuf. Process.* **2022**, *80*, 414–457. [CrossRef]
20. Flynn, J.M.; Shokrani, A.; Newman, S.T.; Dhokia, V. Hybrid additive and subtractive machine tools – Research and industrial developments. *Int. J. Mach. Tools Manuf.* **2016**, *101*, 79–101. [CrossRef]
21. Mordor Intelligence. Hybrid Additive Manufacturing Machine Market—Growth, Trends, and Forecast (2020–2025), Technical Report. Available online: https://www.mordorintelligence.com/ (accessed on 6 March 2023).
22. Demarbaix, A.; Rivière-Lorphèvre, E.; Ducobu, F.; Filippi, E.; Petit, F.; Preux, N. Behaviour of pre-sintered Y-TZP during machining operations: Determination of recommended cutting parameters. *J. Manuf. Process.* **2018**, *32*, 85–92. [CrossRef]
23. *NF E66-520-6*; Working Zones of Cutting Tools. Couple Tool–Material. Association Française de Normalisation AFNOR: Paris, France, 1999.